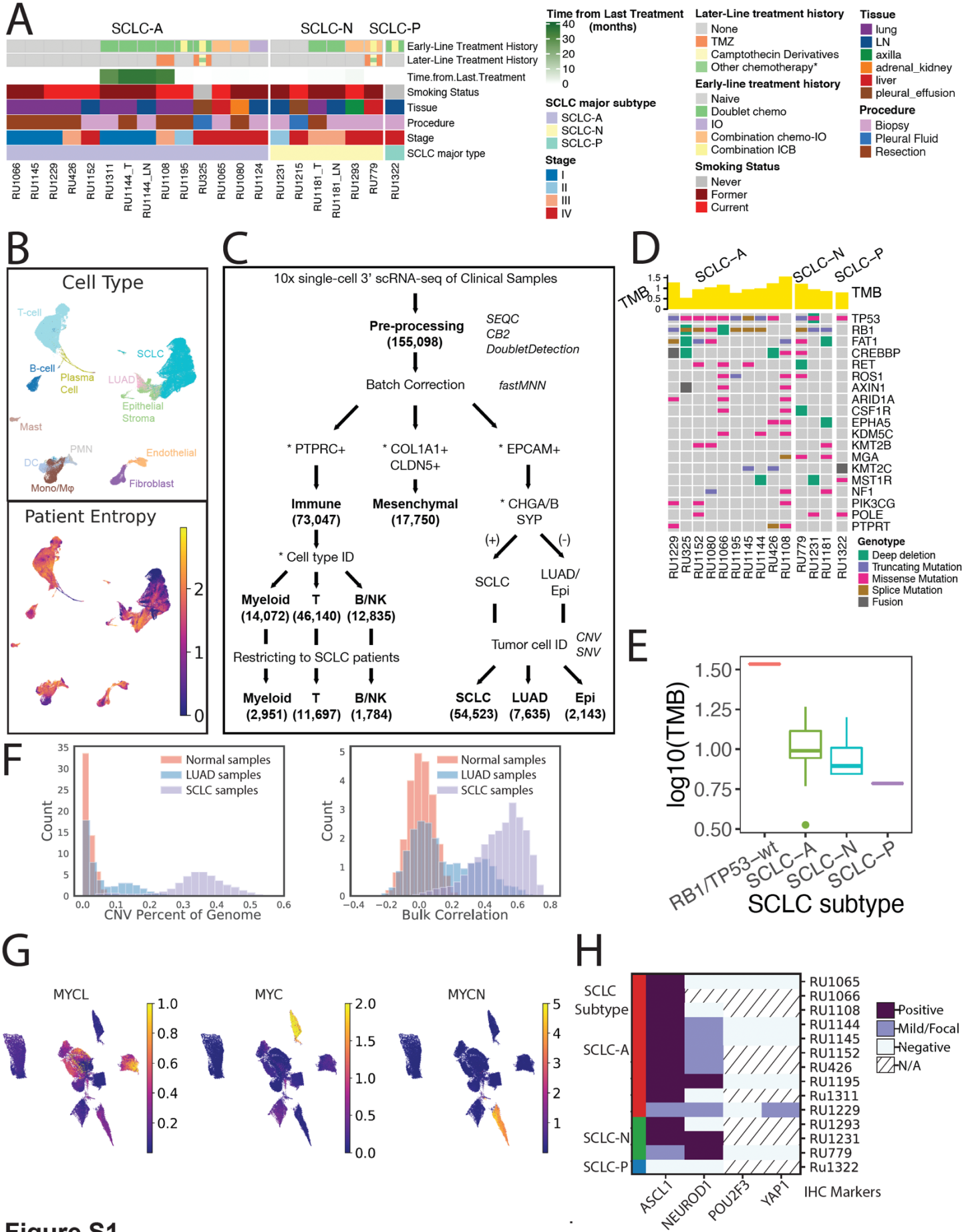
A
SCLC-A
SCLC-N
SCLC-P
Early-Line Treatment History
Later-Line Treatment History
Time.from.Last.Treatment
Smoking Status
Tissue
Procedure
Stage
SCLC major type
RU1066 RU1145 RU1229 RU426 RU1152 RU1311 RU1144_T RU1144_LN RU1108 RU1195 RU325 RU1065 RU1080 RU1124 RU1231 RU1215 RU1181_T RU1181_LN RU1293 RU779 RU1322
Time from Last Treatment (months)
40
30
20
10
0
SCLC major subtype
SCLC-A
SCLC-N
SCLC-P
Stage
I
II
III
IV
Later-Line treatment history
None
TMZ
Camptothecin Derivatives
Other chemotherapy*
Early-line treatment history
Naive
Doublet chemo
IO
Combination chemo-IO
Combination ICB
Smoking Status
Never
Former
Current
Tissue
lung
LN
axilla
adrenal_kidney
liver
pleural_effusion
Procedure
Biopsy
Pleural Fluid
Resection
B
Cell Type
T-cell
B-cell
Plasma Cell
SCLC
LUAD
Epithelial
Stroma
Mast
PMN
DC
Mono/Mφ
Endothelial
Fibroblast
Patient Entropy
2
1
0
C
10x single-cell 3' scRNA-seq of Clinical Samples
Pre-processing (155,098)
SEQC
CB2
DoubletDetection
Batch Correction
fastMNN
* PTPRC+
* COL1A1+ CLDN5+
* EPCAM+
Immune (73,047)
Mesenchymal (17,750)
* CHGA/B SYP
* Cell type ID
(+)
(-)
SCLC
LUAD/ Epi
Myeloid (14,072)
T (46,140)
B/NK (12,835)
Tumor cell ID
CNV
SNV
Restricting to SCLC patients
Myeloid (2,951)
T (11,697)
B/NK (1,784)
SCLC (54,523)
LUAD (7,635)
Epi (2,143)
D
SCLC-A
SCLC-N
SCLC-P
TMB
1.5
1
0.5
0
TP53
RB1
FAT1
CREBBP
RET
ROS1
AXIN1
ARID1A
CSF1R
EPHA5
KDM5C
KMT2B
MGA
KMT2C
MST1R
NF1
PIK3CG
POLE
PTPRT
RU1229 RU325 RU1152 RU1080 RU1066 RU1195 RU1145 RU1144 RU426 RU1108 RU779 RU1231 RU1181 RU1322
Genotype
Deep deletion
Truncating Mutation
Missense Mutation
Splice Mutation
Fusion
E
log10(TMB)
1.50
1.25
1.00
0.75
0.50
RB1/TP53-wt
SCLC-A
SCLC-N
SCLC-P
SCLC subtype
F
Normal samples
LUAD samples
SCLC samples
Count
CNV Percent of Genome
Bulk Correlation
G
MYCL
MYC
MYCN
H
SCLC Subtype
SCLC-A
SCLC-N
SCLC-P
RU1065 RU1066 RU1108 RU1144 RU1145 RU1152 RU426 RU1195 Ru1311 RU1229 RU1293 RU1231 RU779 Ru1322
Positive
Mild/Focal
Negative
N/A
ASCL1
NEUROD1
POU2F3
YAP1
IHC Markers

Figure S1

Figure S1. Related to Figures 1 and 2 and to Table S1.

(A) Clinical attributes of the SCLC cohort in the single-cell atlas (N = 21 tumor samples from 19 patients). Early-line and later-line treatment history is shown in the top two rows with treatment order specified in the order of full square, thin rectangle, and small square. Other annotations include smoking status, tissue, stage, disease status, and SCLC subtype of the major subclone.
(B) UMAP projection of the SCLC cohort at the global level (N=155,098 cells) colored by cell type (top) and by Shannon entropy of patients in a k-nearest neighborhood of each cell (k=30, **STAR Methods**) (bottom).
(C) Flowchart detailing the preprocessing and analytical steps taken at iterative subsets of the single-cell cohort.
(D) Oncoprint showing mutational information for all SCLC samples with matched MSK-IMPACT bulk targeted DNA sequencing available (N = 14 patients), arranged by genes (rows, sorted by most to least recurrent) and patients (columns). Point mutations are depicted by bars, copy number changes by full squares. Bar plot shows tumor mutation burden (TMB).
(E) TMB of SCLC samples, grouped by subtype. Error bars span 25^{th} to 75^{th} percentile.
(F) CNV burden of SCLC, LUAD, and normal lung samples. CNV burden is estimated by percent of genome altered by CNV (left) or Pearson's correlation to CNV profiles of the matched MSK-IMPACT data where available (right). Cancer cells were called based on a threshold of either percent of genome with CNV > 0.1, or bulk correlation $\rho > 0.2$ (**see STAR methods**).
(G) UMAP projection of SCLC cells colored by MAGIC-imputed expression *MYCL* (left), *MYC* (middle), and *MYCN* (right) (**STAR Methods**). Consistent with previous literature (Rudin et al., 2019), we observed that *MYCL* expression was associated with SCLC-A (though one SCLC-N sample, Ru1293, had predominant *MYCL* expression), and that *MYC* expression was relatively low in SCLC-A and highest in the SCLC-P sample (Ru1322) We observed strong *MYCN* expression particularly in one predominant SCLC-N sample (Ru1215).
(H) Heatmap showing immunohistochemistry data available for staining of *ASCL1*, *NEUROD1*, *POU2F3* and *YAP1* transcription factors in the SCLC cohort. Hatched boxes indicate marker staining that was not available due to limited tissue availability. Row annotations indicate the predominant SCLC subtype identified in our scRNA-seq dataset.

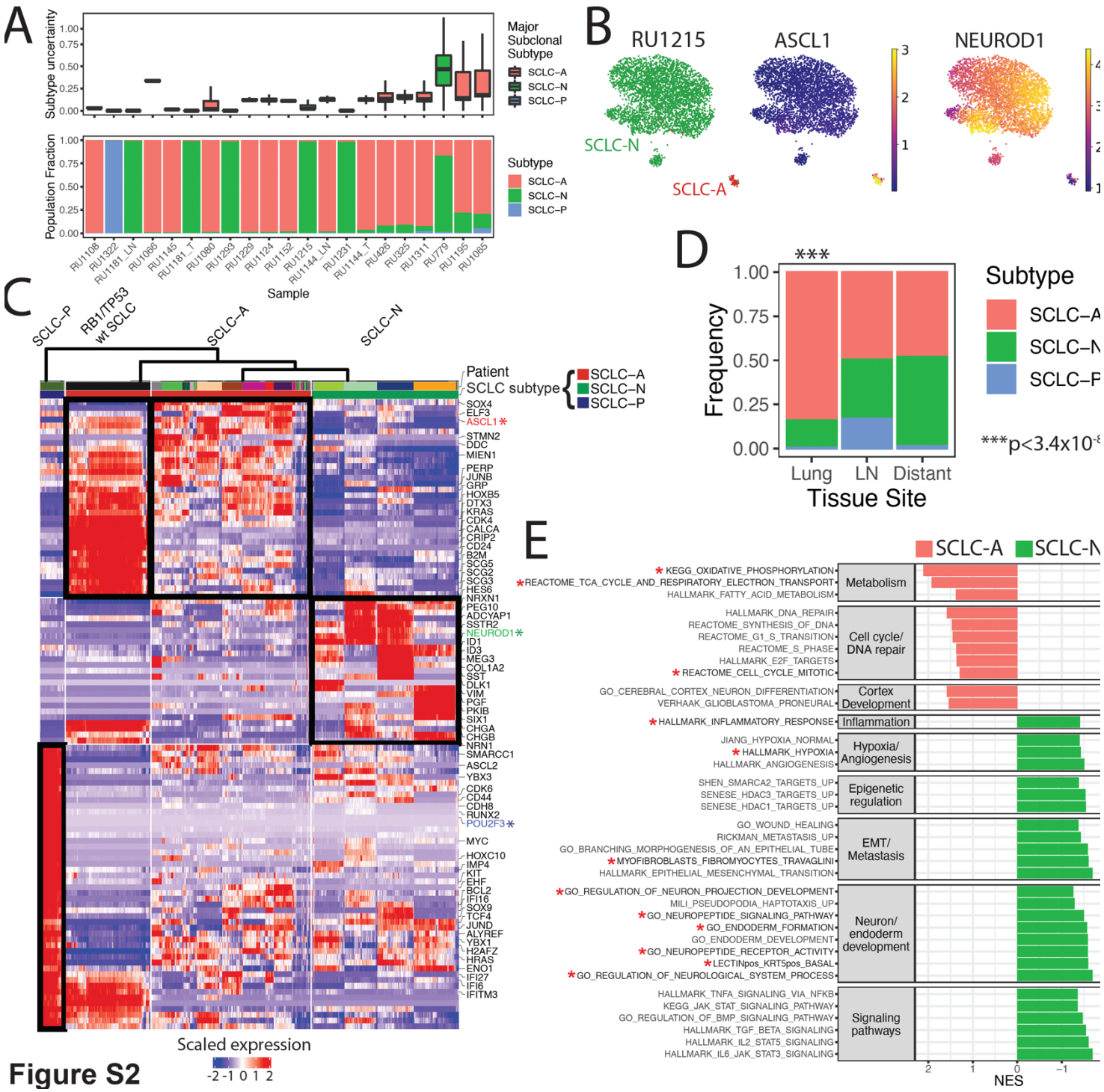

Figure S2

Figure S2. Related to Figures 1 and 2 and to Table S1.

(A) Statistics of SCLC subtype representation in samples (columns). Top: SCLC subtype uncertainty per cell as measured by Shannon entropy of SCLC subtype probabilities. Bottom: SCLC subtype fractions in each sample, as determined by maximum likelihood of Markov absorption probabilities. Error bars span 25th to 75th percentile.

(B) UMAP of sample Ru1215 showing admixed SCLC-A and SCLC-N subtyping, supported by *ASCL1* and *NEUROD1* expression. Cells are colored by maximum likelihood of Markov

absorption probability (left) and MAGIC-imputed gene expression of ASCL1 (middle) and NEUROD1 (right). (**STAR Methods**).
(C) Single-cell gene signatures of SCLC subtypes, with scaled expression (z-score) of differentially expressed genes (DEGs) per SCLC subtype (rows) for each cell (columns). Expression values are imputed using MAGIC (k=30, t=3). Representative DEGs, including canonical TFs are labeled. Top dendrogram produced by hierarchical clustering using Pearson's correlation as a distance metric with complete linkage. Top annotations include patient and SCLC subtype.
(D) Bar plot of frequency of SCLC subtype per tissue site (primary lung vs regional lymph node (LN) vs distant metastasis). The frequency of each subtype per sample was first determined and then summed by tissue site. A final frequency was normalized by the number of samples to produce the stacked bar plot. In this way, each sample was considered with equal weight. SCLC-A was significantly enriched in primary lung, whereas non-SCLC-A subtypes are enriched in nodal and distant metastases (Dirichlet regression, $p<3.4x10^{-8}$, **STAR Methods**).
(E) Gene programs significantly enriched in SCLC-A (red bars) or SCLC-N (green bars) using Gene Set Enrichment Analysis (Benjamini-Hochberg adjusted FDR < 0.05, absolute value of normalized enrichment score (NES) > 1) (**Table S3**). Enriched pathways also confirmed in an independent cohort of bulk RNA-seq are indicated by red asterisks (**STAR Methods**).

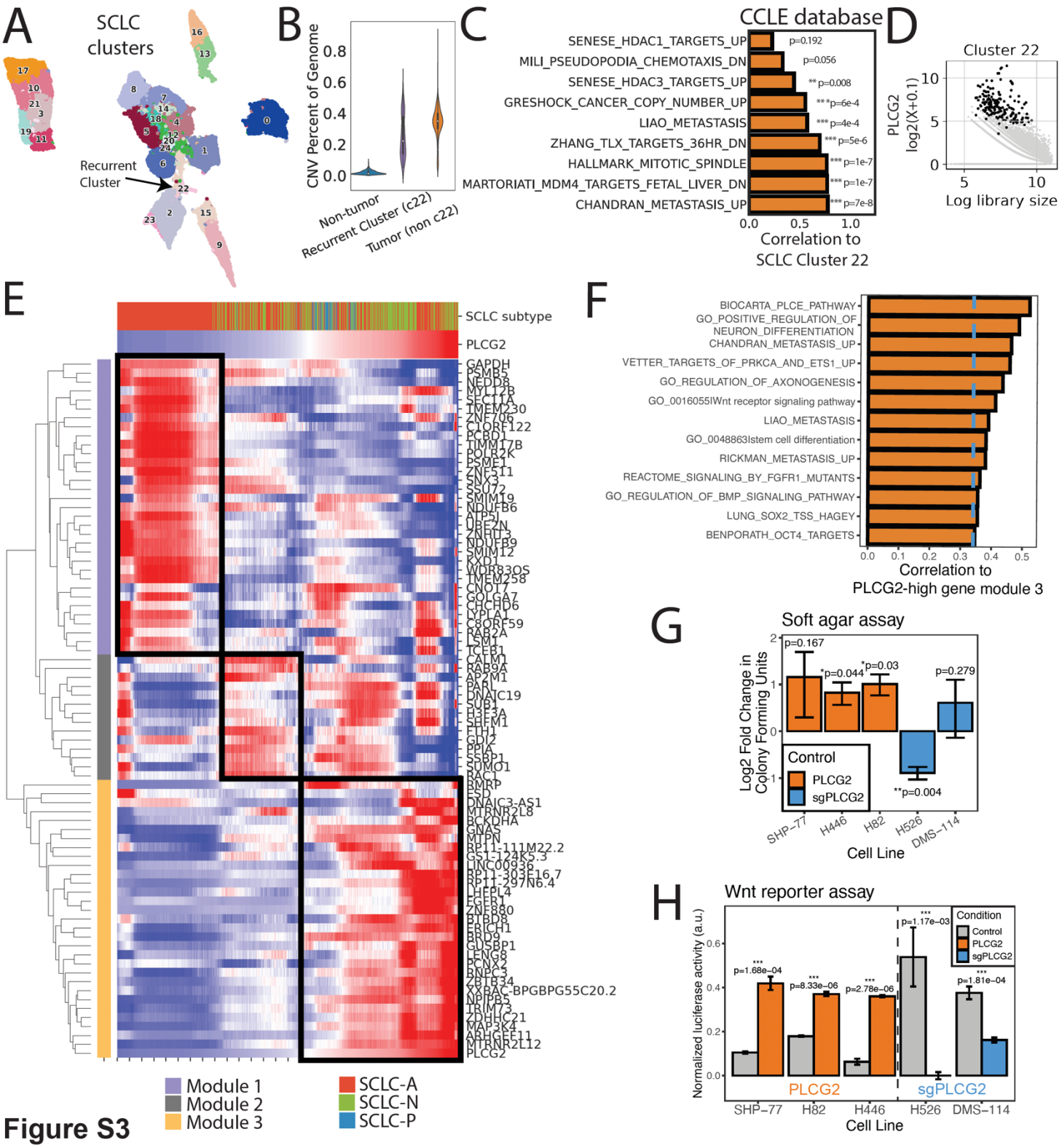

Figure S3

Figure S3. Related to Figures 3 and 4 and to Table S2.

(A) UMAP projection of Phenograph clusters in the SCLC compartment with arrow indicating the recurrent cluster 22.
(B) CNV burden of recurrent cancer cluster 22 compared to normal lung and other SCLC cells.

CNV burden is estimated by percent of genome altered by inferred CNV (**see STAR methods**).
(C) Barplot showing Spearman's correlation of pathways enriched in the recurrent cancer cluster 22 in scRNA-seq to the recurrent cluster gene signature in the CCLE microarray database (N=54; **STAR Methods**).
(D) Unimputed *PLCG2* expression vs log library size in recurrent cluster 22. Library size is transformed by natural log with pseudocount of 1.
(E) Scaled expression (z-score, imputed by MAGIC with k = 30, t = 3) of genes with high knnDREMI conditioned on *PLCG2* > 1 (rows), with cells ordered by *PLCG2* expression (columns). For visualization, expression was smoothed over the ordered cells with a rolling window of 100 cells. Hierarchical clustering of genes on the unsmoothed, imputed expression was performed with complete linkage and Pearson correlation as a distance metric, identifying 3 gene modules that predict low, medium, and high *PLCG2* (purple, gray, and yellow respectively) (**Table S13**). Top annotations include *PLCG2* expression and SCLC subtype.
(F) Pathways with average z-scores of gene expression that are highly correlated (>95th percentile, indicated by blue dashed line) with the average z-score of gene expression in the high-*PLCG2* gene module (**STAR Methods, Table S14**).
(G) Barplot showing log2 fold change in the number of colonies generated by *PLCG2*-overexpressing (SHP77, H446, and H82) and *PLCG2*-KO (H526 and DMS-114) polyclonal cell lines in soft agar colony formation assay, normalizing to the control condition. Error bars: standard deviation.
(H) Barplot showing luminiscence activity of a luciferase Wnt reporter in *PLCG2*-overexpressing (SHP77, H446, and H82) and *PLCG2*-KO (H526 and DMS-114) polyclonal cell lines. Error bars: standard deviation.

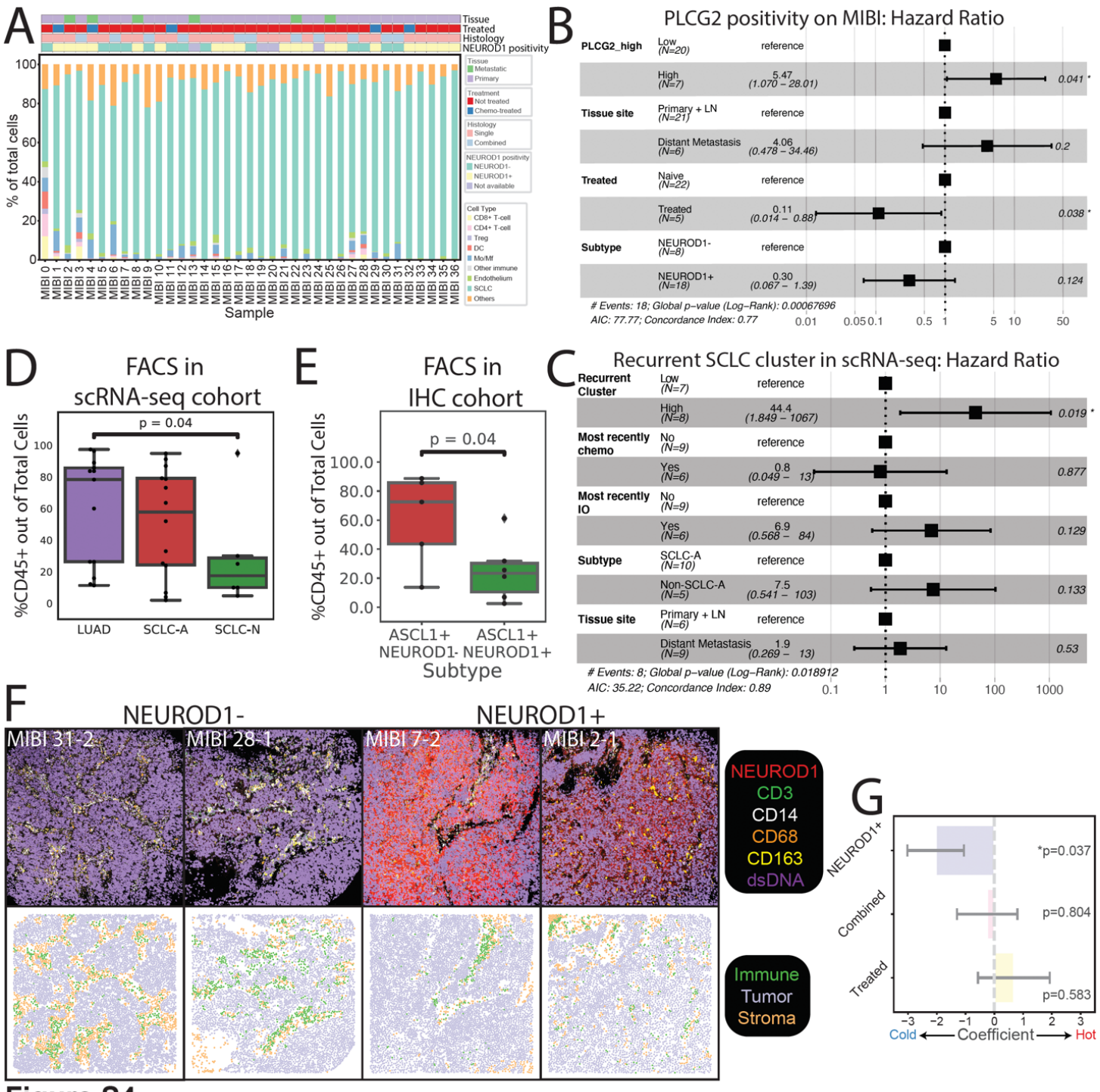

Figure S4

Figure S4. Related to Figure 4 and 5 and to Table S1.

(A) Stacked barplot showing the per-patient abundance of cell types identified by MIBI-TOF.
(B) Multivariate analyses (Cox regression) for overall survival in samples included in an independent cohort of SCLC samples assessed by MIBI-TOF, comparing in patients with high vs

low *PLCG2* positivity (> 7% of SCLC cells, comparing patients with high vs low *PLCG2* positivity (>7% vs ≤7% of SCLC cells with high *PLCG2* staining intensity). The regression model was adjusted for presence of SCLC subtype (classical vs variant), treated with chemotherapy vs naive, and distant metastasis vs primary/regional lymph node. Only samples that were ever extensive-stage (ultimately with metastatic relapse) were considered.
(C) Multivariate analyses (Cox regression) for overall survival in samples included in the single cell cohort, comparing tumors with >0.75% composition of high *PLCG2*-expressing recurrent cluster versus the rest. The regression model was adjusted for presence of SCLC subtype (classical vs variant), most recently treated with chemotherapy alone vs immunotherapy vs naive, and distant metastasis vs primary/regional lymph node. Only samples that were ever extensive-stage (ultimately with metastatic relapse) were considered.
(D) Boxplot of the percentage of CD45+ infiltrate in LUAD vs SCLC-A vs SCLC-N samples in our single-cell cohort (Mann-Whitney test), as assessed by flow cytometry. Error bars: 95% confidence interval.
(E) Boxplot of the percentage of CD45+ infiltrate in an independent cohort of SCLC tumors stratified by SCLC subtype, as assessed by flow cytometry. For SCLC subtype, we compared ASCL1+ NEUROD1- vs ASCL1+ NEUROD1+ samples. No ASCL1- NEUROD1+ samples were available. Differences between conditions were assessed using Mann-Whitney test. Error bars: 95% confidence interval.
(F) Comparison of MIBI images depicting NEUROD1- SCLC tumors (MIBI 31 FoV 2 and MIBI 28 FoV 1 on the left) and NEUROD1+ SCLC tumors (MIBI 7 FoV 2 and MIBI 2 FoV 1 on the right) (each FoV 800 μm by 800 μm), illustrating differences in immune abundance and sequestration. Top: Color overlay of NEUROD1 (red), CD3 (green), CD14 (white), CD68 (orange), CD163 (yellow), and dsDNA (violet) channels. Bottom: FoV from the top now visualized with segmented cancer cells using Mesmer, represented by dots colored by cell type (immune, tumor, and stroma).
(G) Barplot of logistic regression coefficients of 4 covariates (NEUROD1 positivity, combined vs single histology, chemotherapy-treated vs naive, primary vs metastatic) fitted to explain immune hot vs cold tumors (number of immune cells > 250 in a tumor) (Student's t-test). Error bars indicate standard error. Coefficient for primary vs metastatic covariate is not shown due to quasi-complete separation.

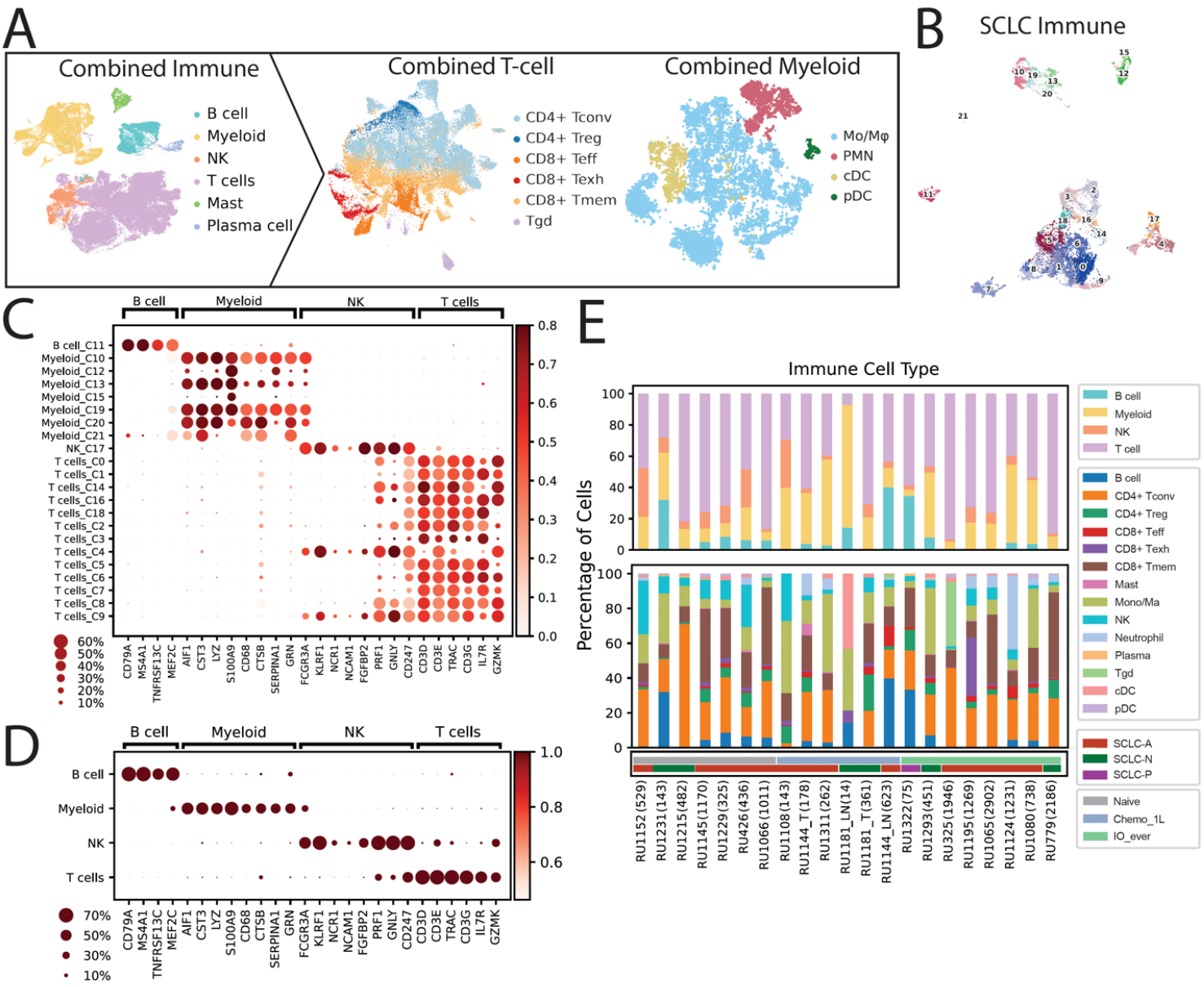

Figure S5

Figure S5. Related to Figure 5 and to Table S15, S16.

(A) UMAP projections of the immune subsets of SCLC with LUAD and adjacent normal lung reference at the global level (top, n=73,047 cells), T-cell compartment (middle, n=46,140 cells), and myeloid compartment (bottom, n=14,072 cells).
(B) UMAP projection of all immune cells from 21 SCLC samples (N = 16,475 cells), annotated by Phenograph clusters.
(C) Dot plots show relative frequency and expressing cells, and mean normalized expression of canonical immune cell type markers per Phenograph cluster.
(D) Dot plots show relative frequency and expressing cells, and mean normalized expression of canonical immune cell type markers per coarse cell type.
PLCG2 = *PLCG2* overexpression, sgPLCG2 = CRISPR knockout.
(E) Stacked barplots of the percentage of coarse immune cell type (top) and fine immune cell type (bottom) in each sample, annotated by SCLC subtype and treatment. Total number of immune cells per sample is indicated in parentheses.

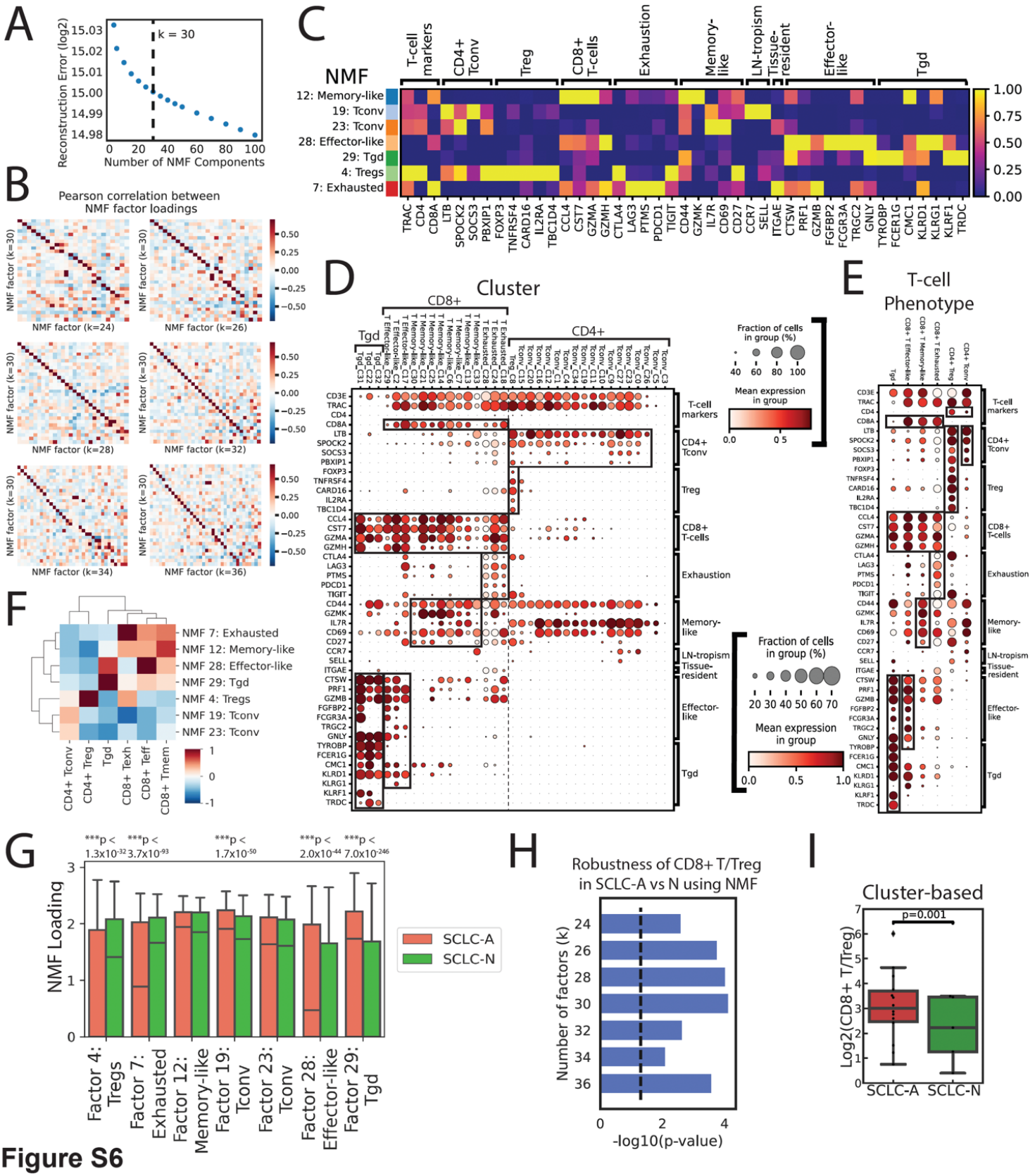
A
Reconstruction Error (log2)
15.03
15.02
15.01
15.00
14.99
14.98
k = 30
0 20 40 60 80 100
Number of NMF Components
B
Pearson correlation between NMF factor loadings
NMF factor (k=30)
NMF factor (k=24)
NMF factor (k=26)
NMF factor (k=28)
NMF factor (k=32)
NMF factor (k=34)
NMF factor (k=36)
0.50
0.25
0.00
−0.25
−0.50
C
NMF
12: Memory-like
19: Tconv
23: Tconv
28: Effector-like
29: Tgd
4: Tregs
7: Exhausted
T-cell markers
CD4+ Tconv
Treg
CD8+ T-cells
Exhaustion
Memory-like
LN-tropism Tissue-resident
Effector-like
Tgd
TRAC CD4 CD8A LTB SPOCK2 SOCS3 PBXIP1 FOXP3 TNFRSF4 CARD16 IL2RA TBC1D4 CCL4 CST7 GZMA GZMH CTLA4 LAG3 PTMS PDCD1 TIGIT CD44 GZMK IL7R CD69 CD27 CCR7 SELL ITGAE CTSW PRF1 GZMB FGFBP2 FCGR3A TRGC2 GNLY TYROBP FCER1G CMC1 KLRD1 KLRG1 KLRF1 TRDC
1.00
0.75
0.50
0.25
0.00
D
Cluster
CD8+
CD4+
Tgd
Fraction of cells in group (%)
40 60 80 100
Mean expression in group
0.0 0.5
T-cell markers
CD4+ Tconv
Treg
CD8+ T-cells
Exhaustion
Memory-like
LN-tropism Tissue-resident
Effector-like
Tgd
Fraction of cells in group (%)
20 30 40 50 60 70
Mean expression in group
0.0 0.5 1.0
E
T-cell Phenotype
CD8+ T Effector-like
CD8+ T Memory-like
CD8+ T Exhausted
CD4+ Treg
CD4+ Tconv
F
NMF 7: Exhausted
NMF 12: Memory-like
NMF 28: Effector-like
NMF 29: Tgd
NMF 4: Tregs
NMF 19: Tconv
NMF 23: Tconv
CD4+ Tconv
CD4+ Treg
Tgd
CD8+ Texh
CD8+ Teff
CD8+ Tmem
1
0
-1
G
***p < 1.3x10-32
***p < 3.7x10-93
***p < 1.7x10-50
***p < 2.0x10-44
***p < 7.0x10-246
NMF Loading
SCLC-A
SCLC-N
Factor 4: Tregs
Factor 7: Exhausted
Factor 12: Memory-like
Factor 19: Tconv
Factor 23: Tconv
Factor 28: Effector-like
Factor 29: Tgd
H
Robustness of CD8+ T/Treg in SCLC-A vs N using NMF
Number of factors (k)
24 26 28 30 32 34 36
0 2 4
-log10(p-value)
I
Cluster-based
p=0.001
Log2(CD8+ T/Treg)
SCLC-A
SCLC-N

Figure S6

Figure S6. Related to Figure 5.

(A) Scatterplot of log2 reconstruction error vs the number of NMF components *k*. The dashed line at k=30 factors represents the kneepoint of the log2 reconstruction error.
(B) Robustness analysis of NMF factors. Heatmaps show correlation between NMF cell loadings identified at k=30 components and over a range of k (24-36).
(C) Heatmap of NMF gene loadings for factors associated with T-cell phenotype. Genes are grouped by T-cell function. Each factor is z-scored across genes, and loadings are subsequently scaled from 0 to 1 across factors (STAR Methods).Dot plots show gene markers of each cluster (D) and T-cell phenotype (E). Dot size = % cells expressing gene; dot color = mean expression scaled from 0 to 1.
(F) Heatmap of cell loading of select NMF factors averaged within each T-cell phenotype based on clusters. The resulting averaged loading was z-scored across factors (**STAR Methods**).
(G) Barplot comparing scaled NMF cell loadings for factors related to T-cell phenotype between SCLC-A and SCLC-N (two-sample t-test adjusted for treatment and tissue site, error bars: 95% confidence interval; **STAR Methods**). *** $p < 0.001$.
(H) Robustness analysis of the decreased CD8+ T/Treg ratio in SCLC-N vs SCLC-A based on NMF. Barplot shows the significance or -log10(p-value) of the difference in ratio between subtypes over a range of k (number of components). (I) Barplot comparing CD8+ Teff/Treg log ratio for based on clusters associated with T-cell phenotype in SCLC-A versus SCLC-N in our single-cell cohort (N=19), adjusted for treatment and tissue site (weighted t-test, error bars: 95% confidence interval; **STAR Methods**).

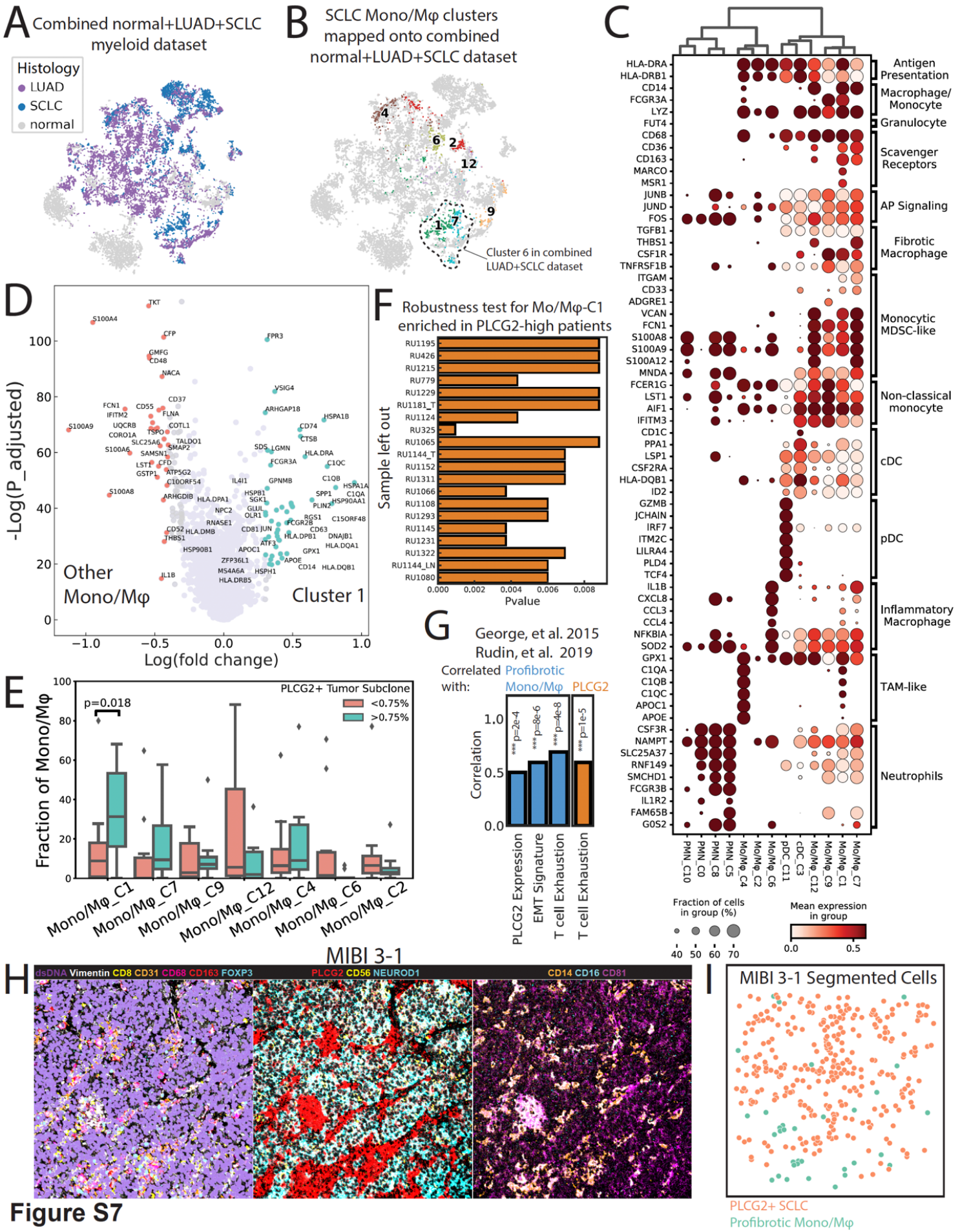
A
Combined normal+LUAD+SCLC myeloid dataset
Histology
LUAD
SCLC
normal
B
SCLC Mono/Mφ clusters mapped onto combined normal+LUAD+SCLC dataset
4
6
2
12
9
1
7
Cluster 6 in combined LUAD+SCLC dataset
C
HLA-DRA
HLA-DRB1
CD14
FCGR3A
LYZ
FUT4
CD68
CD36
CD163
MARCO
MSR1
JUNB
JUND
FOS
TGFB1
THBS1
CSF1R
TNFRSF1B
ITGAM
CD33
ADGRE1
VCAN
FCN1
S100A8
S100A9
S100A12
MNDA
FCER1G
LST1
AIF1
IFITM3
CD1C
PPA1
LSP1
CSF2RA
HLA-DQB1
ID2
GZMB
JCHAIN
IRF7
ITM2C
LILRA4
PLD4
TCF4
IL1B
CXCL8
CCL3
CCL4
NFKBIA
SOD2
GPX1
C1QA
C1QB
C1QC
APOC1
APOE
CSF3R
NAMPT
SLC25A37
RNF149
SMCHD1
FCGR3B
IL1R2
FAM65B
G0S2
Antigen Presentation
Macrophage/ Monocyte
Granulocyte
Scavenger Receptors
AP Signaling
Fibrotic Macrophage
Monocytic MDSC-like
Non-classical monocyte
cDC
pDC
Inflammatory Macrophage
TAM-like
Neutrophils
PMN_C10
PMN_C0
PMN_C8
PMN_C5
Mo/Mφ_C4
Mo/Mφ_C2
Mo/Mφ_C6
pDC_C11
cDC_C3
Mo/Mφ_C12
Mo/Mφ_C9
Mo/Mφ_C1
Mo/Mφ_C7
Fraction of cells in group (%)
40 50 60 70
Mean expression in group
0.0 0.5
D
-Log(P_adjusted)
Log(fold change)
Other Mono/Mφ
Cluster 1
TKT
S100A4
CFP
FPR3
GMFG
CD48
NACA
VSIG4
CD37
FCN1
CD55
FLNA
IFITM2
ARHGAP18
HSPA1B
S100A9
UQCRB
COTL1
CD74
CORO1A
TSPO
CTSB
SLC25A6
TALDO1
SMAP2
SDS
LGMN
S100A6
SAMSN1
HLA.DRA
LST1
CFD
FCGR3A
C1QC
GSTP1
ATP5G2
C10ORF54
IL4I1
GPNMB
C1QB
HSPA1A
S100A8
ARHGDIB
HLA.DPA1
HSPB1
SGK1
SPP1
C1QA
HSP90AA1
NPC2
GLUL
OLR1
PLIN2
RGS1
C15ORF48
RNASE1
FCGR2B
CD52
HLA.DMB
CD81
JUN
CD63
THBS1
HLA.DPB1
DNAJB1
ATF3
HLA.DQA1
HSP90B1
APOC1
GPX1
ZFP36L1
APOE
CD14
HLA.DQB1
MS4A6A
HSPH1
IL1B
HLA.DRB5
E
Fraction of Mono/Mφ
PLCG2+ Tumor Subclone
<0.75%
>0.75%
p=0.018
Mono/Mφ_C1
Mono/Mφ_C7
Mono/Mφ_C9
Mono/Mφ_C12
Mono/Mφ_C4
Mono/Mφ_C6
Mono/Mφ_C2
F
Robustness test for Mo/Mφ-C1 enriched in PLCG2-high patients
Sample left out
RU1195
RU426
RU1215
RU779
RU1229
RU1181_T
RU1124
RU325
RU1065
RU1144_T
RU1152
RU1311
RU1066
RU1108
RU1293
RU1145
RU1231
RU1322
RU1144_LN
RU1080
Pvalue
G
George, et al. 2015
Rudin, et al. 2019
Correlated with:
Profibrotic Mono/Mφ
PLCG2
Correlation
*** p=2e-4
*** p=8e-6
*** p=4e-8
*** p=1e-5
PLCG2 Expression
EMT Signature
T cell Exhaustion
T cell Exhaustion
MIBI 3-1
H
dsDNA Vimentin CD8 CD31 CD68 CD163 FOXP3
PLCG2 CD56 NEUROD1
CD14 CD16 CD81
I
MIBI 3-1 Segmented Cells
PLCG2+ SCLC
Profibrotic Mono/Mφ

Figure S7

Figure S7. Related to Figures 6 and 7.

UMAP projections of combined myeloid compartment (SCLC, LUAD, and normal adjacent lung), annotated by (A) tumor histology and (B) Mono/Mφ clusters identified from the SCLC-restricted myeloid compartment. In (B), the dashed outline indicates cells identified as cluster 6 in the clustering of the combined myeloid dataset of SCLC and LUAD samples.
(C) Dot plot of SCLC myeloid subsets and expression of relevant markers. Myeloid subsets are ordered based on hierarchical clustering of the first 50 principal components (**STAR Methods**). Dot size = % cells expressing gene; dot color = mean expression scaled from 0 to 1.
(D) Volcano plot of differentially expressed genes in SCLC Mono/Mφ cluster 1 of the SCLC myeloid compartment versus other Mono/Mφ subsets (**Table S20**).
(E) Boxplots showing the composition of Mono/Mφ clusters stratified by PLCG2+ SCLC subpopulation comprising > 0.75% of cancer cells within each tumor. Mono/Mφ clusters are arranged along the X-axis in order from high to low score for IPF-associated Mono/Mφ (shown in Fig. 7C). We show significant overrepresentation of Mono/Mφ cluster 1 in samples harboring the recurrent PLCG2-high SCLC subpopulation. Error bars: 95% confidence interval.
(F) Bar plot showing robustness of covariate-adjusted Spearman correlation p-values using leave-one-sample-out cross-validation.
(G) Barplot showing Spearman's correlation of the profibrotic Mono/Mφ gene signature to *PLCG2* expression, EMT, and T-cell exhaustion gene signatures, as well as *PLCG2* to T-cell exhaustion, in published bulk RNA-seq datasets from George, et al. 2015 and Rudin, et al. 2019 (N=81; **STAR Methods**).
(H) Color overlay of SCLC tumor MIBI 3 at FoV 1 (size 500 μm x 500 μm) showing the co-occurrence of the PLCG2-positive SCLC cells and the putative profibrotic Mono/Mφ, similar to MIBI 12 at FoV 1 in Figure 7C. Left: Channels dsDNA (violet), Vimentin (white), CD8 (yellow), CD31 (orange), CD68 (red), CD163 (red), and FOXP3 (cyan) illustrate the global tumor environment structure. Middle: Channels PLCG2 (red), CD56 (yellow), and NEUROD1 (cyan) illustrate PLCG2+ tumor. Right: Channels CD14 (orange), CD16 (cyan), and CD81 (magenta) illustrate the putative profibrotic Mono/Mφ.
(I) FoV from the (H) now visualized with segmented cancer cells using Mesmer, represented by dots colored by PLCG2+ SCLC cells vs profibrotic Mono/Mφ.